Chapter 4

Thermo-Foaming Technique via Sucrose Dehydration Process

The contents of this chapter have appeared as:

"Synthesis, morphological and thermomechanical characterization of light weight silica foam via reaction generated thermo-foaming process"

Vaibhav Pandey, Mayank Kumar Yadav, Ashutosh Gupta, Kalyani Mohanta, S.K. Panda, V.K. Singh,

Journal of the European Ceramic Society 42 (**2022**) 6671–6683

https://doi.org/10.1016/j.jeurceramsoc.2022.07.034

4.1 Introduction

The previous chapter successfully demonstrated the effectiveness of the novel Alumina dissolution process for fabricating porous composites with the capability to create complex geometries through green machining, facilitated by the excellent green strength obtained through this process. However, it is important to acknowledge that this process has certain limitations. Firstly, it is limited to compositions that either already have alumina content or require the addition of alumina to develop such porous structures. Secondly, the process is constrained to porous structures with a maximum porosity of 70%, which restricts the ability to achieve ceramic foam composites. These limitations hinder the process from forming porous structures using all types of ceramic powders. To address this, there is a need to develop an alternative process capable of producing highly porous ceramics, specifically ceramic foams, which can be applicable to a wider range of ceramics.

Chapter 2 provides an in-depth exploration of the distinctive intrinsic properties of ceramic foams, along with their suitable applications and diverse preparation methods. However, there is a need to bridge a gap in the literature by investigating and developing a novel technique specifically aimed at achieving ceramic foams. This chapter will address this gap by focusing on the exploration of innovative techniques for fabricating ceramic foams. The objective is to develop a new method that overcomes the limitations of existing processes and allows for the production of highly porous ceramic foams.

In the ceramic foaming process, sucrose has been widely studied either as a foaming agent or as an abetting agent for other foaming materials [117–124]. Prabhakaran et al. have [119] developed a new processing route to develop alumina foam using sucrose as a foaming agent. Aluminum nitrate was used to prepare sucrose resin. Alumina slurry was mixed and heated at higher temperatures to get desired foaming effect. Similarly, Ji et al. [125] used sucrose, kaolinite clay and aluminium nitrate to generate carbon foams by applying thermo-foaming method. Alumina foam having 98.5 % porosity was prepared by Ganesan et al. [121] using sucrose and aluminium nitrate. Similarly, the effect of alumina to sucrose weight ratio on foaming properties had been studied by employing sucrose as a foaming material [124]. One can also find the use of sucrose in the preparation of carbon black [126]. Sucrose, an excellent source of carbon was extensively used to produce carbon using various chemical processes. Dehydration of sucrose with oil of sulphuric acid (H_2SO_4) was also employed for the carbonization of sucrose, thereby turning sucrose into a porous carbon scaffold [127].

However, above discussed state of the art literatures did not see the possibility of sucrose dehydration to develop ceramic based porous scaffolds. Considering the wide range of application of such materials, this work focuses on a novel synthesis route to fabricate high porosity ceramic foam with promising thermomechanical properties. The remarkable foaming, binding and rheological properties of low-cost ingredients like sucrose and oil of vitriol have been synergized to prepare the ceramic scaffold specimens. To assess the characteristics, detailed microstructural analyses such as SEM, TEM and Micro CT have been carried out. Thermoelastic properties are compared at various sintering temperatures. The mentioned thermo-foaming process not only provides a simple and low-cost approach to fabricate ceramic foam but also have the ability to produce gradient microstructures.

Silica, one of the most abundant oxides in the earth's crust, is a widely studied material due to its intrinsic properties and availability. It finds applications in microelectronics, structural materials and as components in the food and pharmaceutical industries. Porous silica ceramics are also found to be ideal candidates for the filter, adsorbent, acoustic and thermal protection applications [128–135]. Table 4.1 provides details of some of the published works of porous silica/ silica composites with their applications. Considering the enormous demand of porous silica, silica powder has been chosen as a precursor material for conducting experiments and establishing foaming techniques.

The procedure outlined in the subsequent sections elaborate on fabrication method, optimization of constituents for a better product and subsequently their microstructure and mechanical characterization. Initially, the amount of sulphuric acid for the ceramic slurry preparation is determined after several trial-and-error configurations for best green foam. A systematic casting and foam setting method has been followed in this work to obtain the high porosity silica foam. Effect of sucrose to ceramic weight ratio on the microstructure of foam and thermomechanical properties has also been studied for the characterization of ceramic foam. The properties obtained encourage using this low-cost alternative fabrication route to prepare high volume porous ceramic foam.

4.2 Materials and Method

4.2.1 Raw materials

Fine silica powder procured from LOBA Chemie Pvt. Ltd. is the basic ingredient for preparing the ceramic foam. Concentrated sulphuric acid (98 wt%) (oil of vitriol) and sucrose used are of analytical reagent grade (Merck, India). Sucrose acts as fugitive material as well as a blowing

agent. The cost-effectiveness can be related to the price per kg, which comes around a few hundred rupees for ingredients, where reagents like sucrose are only 1-20 wt% of silica foam prepared.

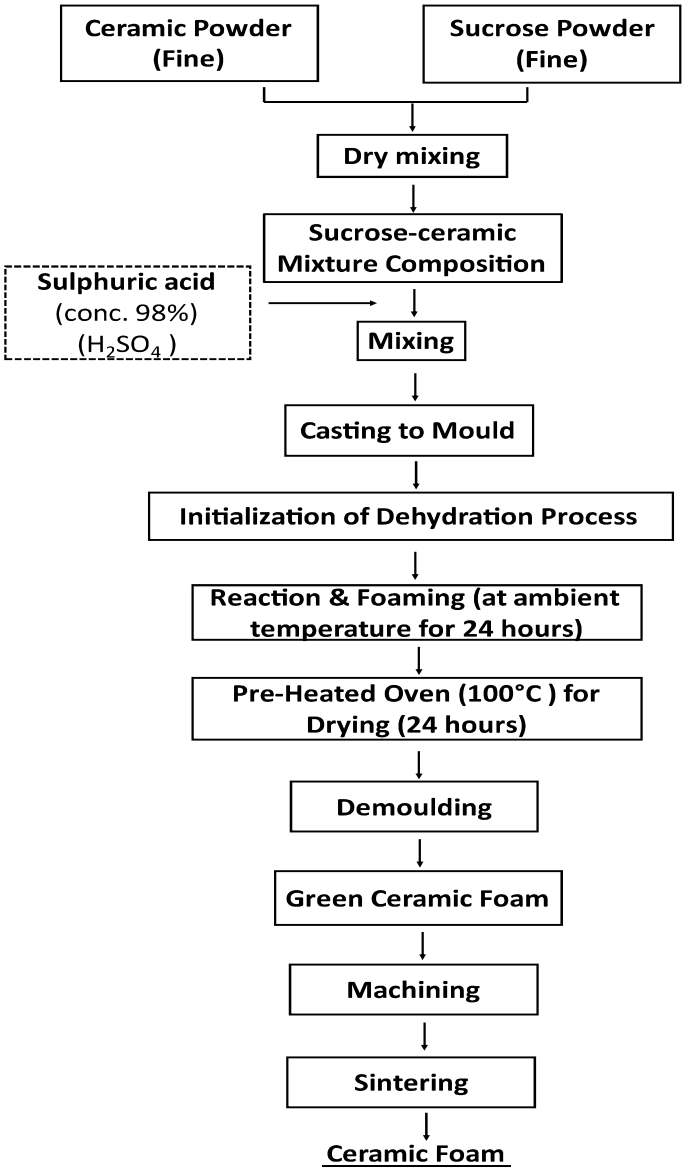

Fig. 4.1 Standard process flow chart of fabrication of silica foam

4.2.2 Fabrication procedure

Fig. 4.1 delineates the schematic of this work to prepare the sintered silica foam. The fabrication process of silica foam involves mixing fine sucrose powder with fine silica powder. Different ceramic compositions are prepared by mixing sucrose to silica powder as per the stated weight ratio of 0.01–0.20. Hereafter sucrose to silica weight ratio is denoted as $W_{Su/Si}$ ratio. Ceramic slurry with 60 wt% solids loading has been prepared by adding concentrated sulphuric acid into the ceramic mixture. Solids loading is optimized by considering the

minimum amount of sulphuric acid required to complete the dehydration process of sucrose as well as making the slurry viscous enough so that it can be easily foamed without any hindrance or distortion. Otherwise, very high viscous slurry might not expand properly affecting the foaming process itself. Ceramic slurry is thoroughly mixed so that ceramic mixture particles are dispersed uniformly into the sulphuric acid. After proper mixing of slurry, casting of slurry is carried out with the appropriate cast and left for 24 h for foaming at ambient atmosphere (around 30-40°C). Foaming process is followed by drying in a pre-heated oven of 100°C for 24 h. Mixing and casting have been done fast after pouring sulphuric acid into the powder mixture so that the dehydration should start immediately after loading into the cast. Specific attention should be given to the selection of cast in order that it should not be reactive to sulphuric acid. After foaming and drying, green foams are removed from the cast and cut into the required shape and size. Calcinations of green silica foam are done at a temperature of around 1000°C to remove the carbon, fugitive material and any other impurities. Calcinations also provide better strength to the silica foam for handling, which is again subjected to sintering process in the range of 1300-1600°C to get the final product.

4.2.3 Characterization

Physical and chemical changes during the pre and post dehydration process are studied by Fourier-transform infrared spectroscopy (FTIR) and Transmission electron microscopy (TEM) analysis. FTIR provides the difference in the vibrational mode of silica and silica-sucrose composition due to the dehydration reaction for both green samples and the sintered samples after the sintering process. The attenuated total reflection (ATR) method using KBr pellet over the wavenumber range of 4000-500 cm^{-1} is used to carry out FTIR analysis (BRUKER (Yokohama, Kanagawa, Japan), TENSOR 27-3772)). Similarly, microstructural changes are recognised by a high-resolution transmission electron microscope (HRTEM, FEI, TECNAI G2–20 TWIN, Eindhoven, Netherlands) at an accelerating voltage of 300 kV. The thermal decomposition of H_2SO_4 treated silica-sucrose mixture has been studied by Thermogravimetric analysis (TGA) (TGA-50, Shimadzu (Asia Pacific) Pte Ltd). The TGA measurements have been conducted within an atmospheric air environment at a heating rate of 3°C/min. The XRD measurements of synthesised silica foam are examined through an X′ Pert Pro diffractometer equipped with Cu-kα (1.5406 Å) radiation as the X-ray source, in the 2θ range of 10°-110° with a step size of 0.02°. The surface morphology and microstructure analyses have been carried out with the help of a Scanning Electron Microscope (SEM) (ZEISS, Jena, Germany, EVO 18-2045). SEM microstructures taken at low magnification are used to calculate the average pore

size of silica foams for at least four randomly selected locations on each sample using the Planimetric (or Jeffries') procedure described in ASTM E112-13 [36]. Percentage of test area occupied by each phase is determined by practice E562-19 [37]. An image analysis software (Version 1.53i, U. S. National Institutes of Health, Bethesda, Maryland, USA) [38] has been used to calculate average pore size using SEM micrographs. In order to have a better understanding of microstructure, pore morphology and its size distribution, Micro-computed tomography (μCT) analysis of polished silica foam sintered at 1600°C is carried out using the SkyScan1076 CT scanner (Aartselaar, Belgium). The cuboidal shape specimen (length=15 mm, breadth=10 mm & height=10 mm) is vertically mounted on the stage and analysed using an X-ray source at a voltage of 86 kV and a current of 110 mA. During the analysis, images are obtained at a rotation step of 0.1°, and reconstructed images are obtained by SkyScan's volumetric NRecon reconstruction software. The bulk density and total porosity are calculated using standard test methods, while open porosity is calculated by the water immersion based on Archimedes' displacement method. As per ASTM C1161-18, bending samples are prepared meticulously, as shown in Fig. 4.2. The dimension and ratios are checked with a digital Vernier calliper. A crosshead speed of 0.2 mm/min is set up after some trial run in the computerized test method of the Universal Testing Machine (INSTRON) [136]. For the bending testing, porous silica cylinders of 15 mm diameter and 30 mm thickness have been prepared. Five test specimens from each category of slurry loadings and corresponding sintering temperature are tested for the purpose of estimating a mean. TPS-500, Goteborg, Sweden, made Hot Disk instrument has been used to measure the thermal conductivity of the porous silica. Measurements are taken by sandwiching the hot disk sensors between two identical silica foam pieces. The sensor system has an electrically conducting pattern in the shape of a double spiral laminated between two thin sheets of insulating material (Kapton).

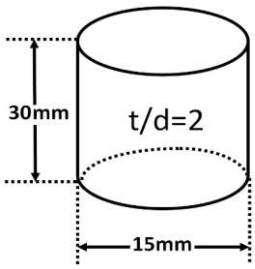

Fig. 4.2 Schematic of specimen used for compression testing as per ASTM standard

Table 4.1 Silica and silica based porous composites with proposed application.

Compositions	Proposed application
Porous silica composite reinforced with polysiloxane [137]	Thermal insulation
Porous silica [138]	Lightweight and low dielectric materials
Silica/mullite porous ceramic [139]	Thermal insulation
Porous silica ceramics [140]	Thermal insulation
3-glycidoxyproyltrimethoxysilane- gelatin-silica hybrid scaffolds[141]	Bone scaffold
Porous Silica-Silicon nitride composite [142]	Acoustic insulators
Porous Silica- composites with various additives [143]	Thermal insulation
Silica-alumina-calcium and iron based porous composite [129]	Phosphorus removal
Silica-based TODGA impregnated porous adsorbent [130]	Adsorption and separation of Y(III) and Sr(II) in acid solution
Porous silica [131]	Removal of tar components generated fromwaste biomass
Porous silica gel [132]	Adsorbent in the controlled drug delivery systems
Vinyl-modified porous silica[133]	Catalysis and separation
Paraffin/porous silica ceramic composite[134]	Thermal insulation
Porous silica [135]	Siloxane adsorption

4.3 Results and Discussion

4.3.1 Foam synthesis mechanism

When sulphuric acid is mixed with sucrose-silica mixture composition, there is a delay of almost one minute before the start of the reaction. After a while, acid starts yellowing due to dehydration of sucrose. Delay in the reaction helps in forming silica slurry and facilitates proper mixing and adhering of sucrose with silica powder. Sucrose adhering is also attributed to the interaction of hydroxyl groups of sucrose with silica particle surface. The optimized amount of sulphuric acid makes the slurry viscous enough to wet the sucrose-silica mixture and prohibit the excess flow. The reaction accelerates as the acid heats up due to the hydration of sulphuric acid and dehydration of sucrose, as both are exothermic processes. During the reaction, sucrose breaks down into carbon and water molecules, and the carbon agglutinates on the silica particles. TEM study confirms the morphological changes in the surface of silica particles due to the dehydration reaction of silica-sucrose composition with sulphuric acid. Figure 4.3(a)

show irregular, big and non-homogeneous particles of silica, before reaction [144] and black colour spots (Fig. 4.3-(b)) can be easily seen over the entire surface of silica particles, after the dehydration process. These black colour coating observed is due to the agglutination of carbon particles over silica particles [145]. This carbon further reacts with the remaining H_2SO_4 to form water vapour, carbon dioxide and silicon dioxide gases. These gases exert pressure thereby foaming the slurry. Ultimately, they escape from the slurry by creating a porous skeleton of carbon-coated silica (Fig. 4.4).

$$C_{12}H_{22}O_{11}\ (s) \rightarrow 12\ C\ (s) + 11\ H_2O\ (l)$$

$$C + 2\ H_2SO_4 \rightarrow CO_2(g) + 2\ SO_2(g) + 2\ H_2O(g)$$

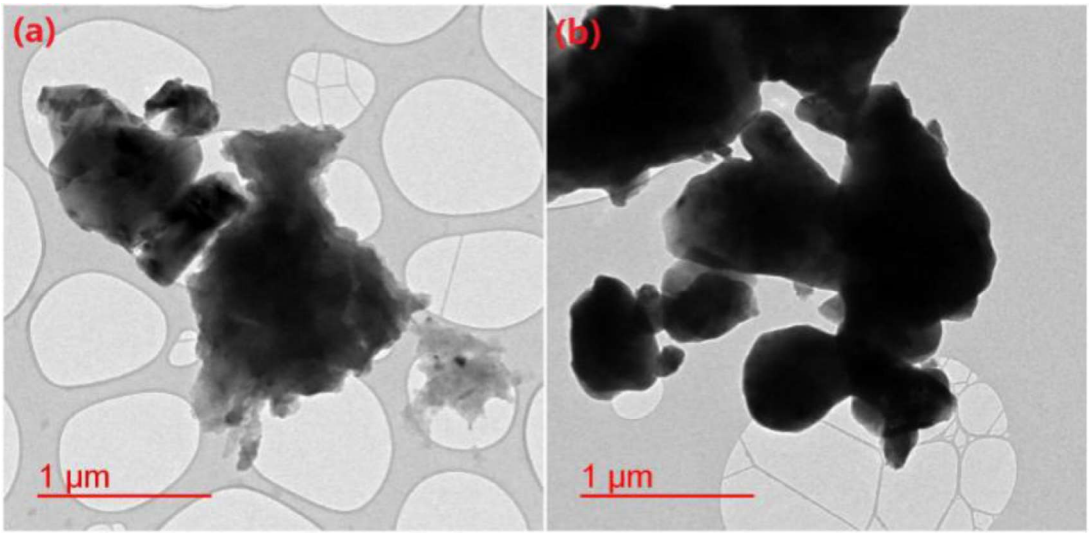

Fig. 4.3 TEM image of (a) SiO_2 particles (b) Carbon coated silica particles

Fig. 4.5 shows the image of green silica foam with optical image of their surface. It is clearly evident from the optical image that green silica foam has 3D network structure of carbon coated silica. The porous scaffold so obtained is due to formation of 3D connected network of carbon which arises due to foaming reaction between sucrose and sulphuric acid. However, it is found that stability of the green foams is dependent on the slurry rheology. During the experiments, it was found that when high viscous slurry was used, there was no concrete foaming, irrespective of the fact that sucrose has the ability to form a stable three-dimensional connected carbon framework without the addition of any ceramic particle. It was observed that foaming was difficult too with low viscous slurry and it collapses due to gravitational pull of slurry which weakens the green foam strength. This collapse of green structure couldn't be saved

even with the support of three-dimensional connected carbon framework. Hence, from these observations it can be concluded that the three-dimensional connected carbon framework does not help much in maintaining the shape of green foam, rather help in creating the foam.

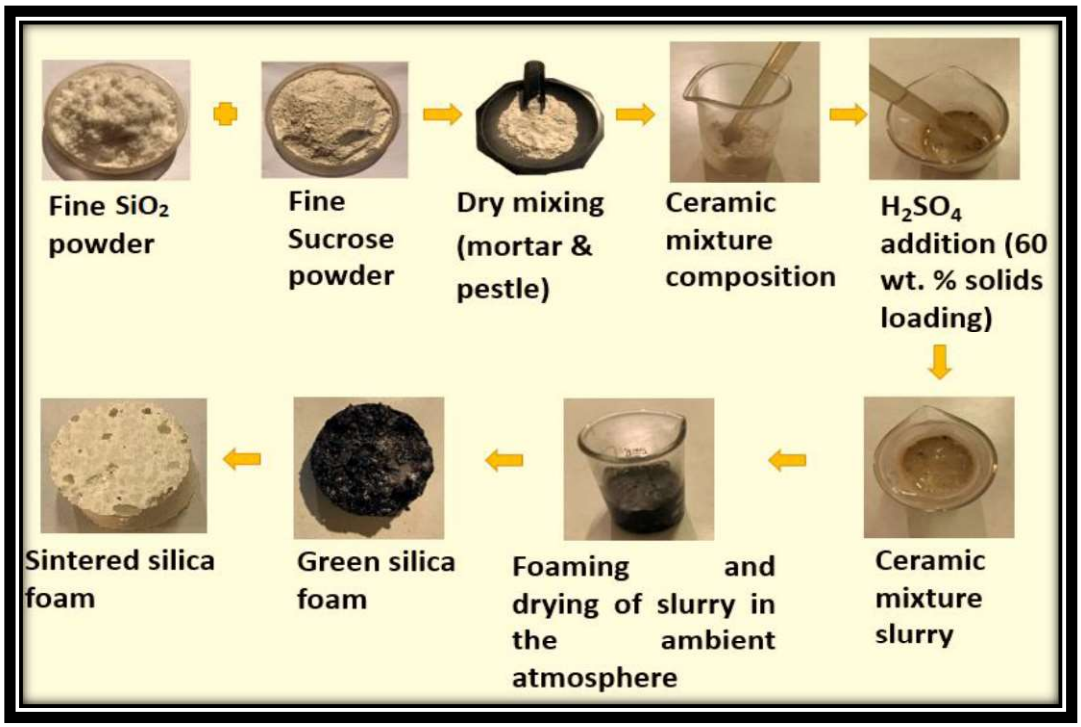

Fig. 4.4 Pictorial representation of fabrication of silica foam

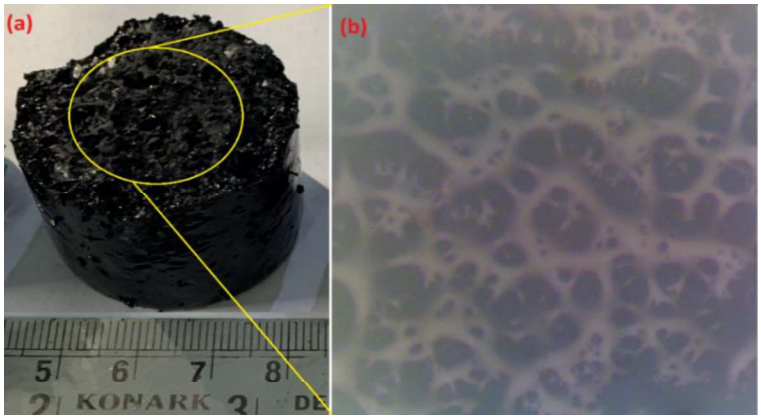

Fig. 4.5 Figure showing (a) green silica foam and (b) Optical image of the green silica foam

Foaming of slurry increases with an increase in sucrose amount. It has been observed that uniform and controlled foamed structures formed up to 0.2 $W_{Su/Si}$ ratio. Beyond this ratio, extreme pressure is created in the slurry due to excess production of escaping gases. This generates a non-uniform structure reducing the foam strength due to thinning of the strut and

pore walls. High viscous slurry foaming is either complex or else this happens with gradient foaming. Contrastingly, low viscous slurry results in imbalanced or unstructured porous configurations intending the collapse of the structure. Figure 4.6 shows a linear trend in foaming behaviour with respect to $W_{Su/Si}$ ratio. Significantly, there is a considerable increase in the height of the green foam (almost doubled) when this weight ratio is increased from 0.01 to 0.2.

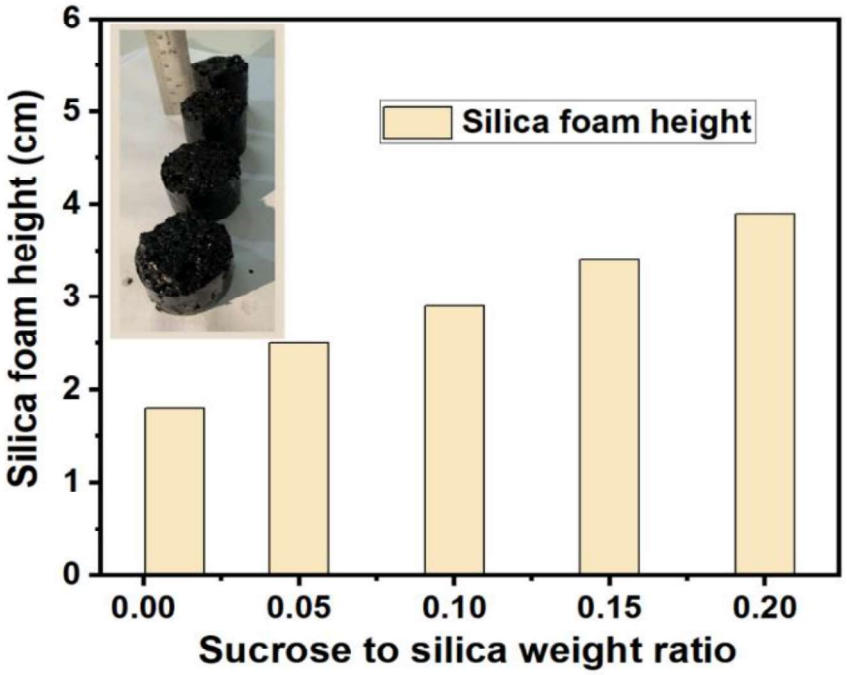

Fig. 4.6 Effect of $W_{Su/Si}$ ratio on foaming height

The green foam obtained with the optimized slurry composition, possesses excellent handling strength and can sustain minor machining operations. The TG analyses of green foams show the weight loss in three stages between 50°C to 500°C (Fig. 4.7). Due to the escape of water vapour, significant weight loss is observed within temperature range of 50°C-150°C. A comparatively steady loss of produced carbon owing to dehydration of sucrose follows in the second stage between 180°C-240°C. At the last stage between 400°C-500°C, oxidation causes removal of other impurities. TG analysis provides an idea about the heat treatment schedule for removing organic impurities. A slow and steady heating rate of 3°C/minute is followed up to 600°C to remove all the organic impurities present in the green silica foam, followed by sintering process. This has been scheduled between 1300°C to 1600°C at the rate of 5°C/minute.

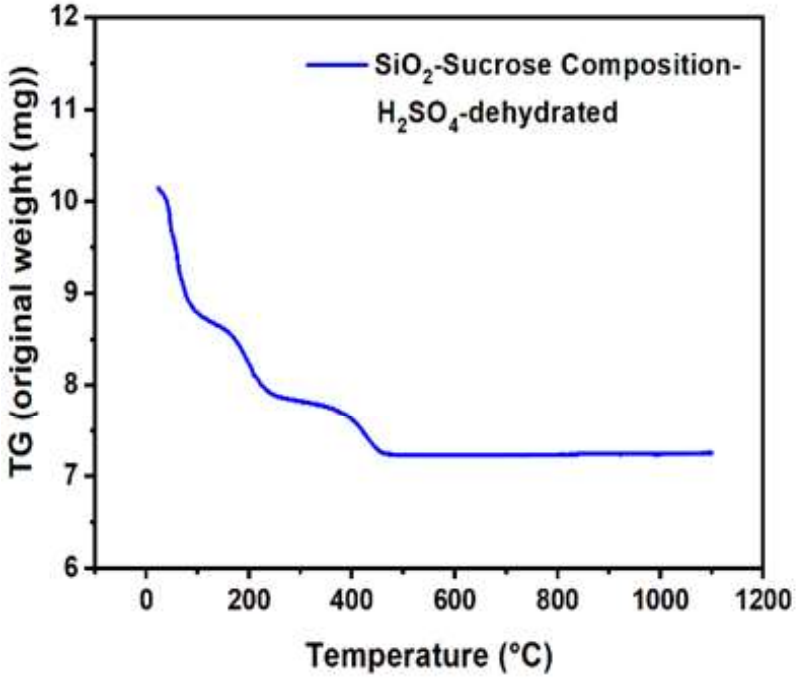

Fig. 4.7 TG analysis of H_2SO_4 treated silica-sucrose mixture (Green Foam)

Green foams with varying compositions are further heat treated for final consolidation of ceramic and providing sufficient strength to foams. Figure 4.8 shows the XRD pattern of sintered silica foam. The patterns are noted in the 2-theta (2θ) range from 5° to 110°. Sharp peaks are observed at 20.869°, 21.906°, 26.643°, 36.532°, 39.456°, 40.278°, 42.565°, 45.912°, 50.118°, 54.863°, 59.934° with interlayer spacing [d- spacing (Å)] of 4.25, 4.05, 3.34, 2.45, 2.283, 2.239, 2.127, 1.979, 1.818, 1.672, 1.542 Å respectively. The XRD pattern confirms the presence of SiO_2 with different phases. Most of the peaks are of quartz phase, with intense peaks at 26.643°. Peaks of cristobalite and tridymite phase are also evident but comparatively at a lesser intensity. The XRD pattern gives a clear view of the existence of a single compound (SiO_2) with multiple phases confirming the removal of any organic impurities during sintering. No cracking or deformation is observed during calcination and sintering. Noticeable shrinkage is observed at higher temperatures inflicting decrease in porosity. It is well known that shrinkage of pore is sintering-temperature dependent. Figure 4.9 shows silica foams sintered at 1500℃ with a cross-section showing their pore distribution pattern. The pattern shows macropores visible through naked eyes, resembling Yellow Jacket's nest containing multiple layers of spherical cells.

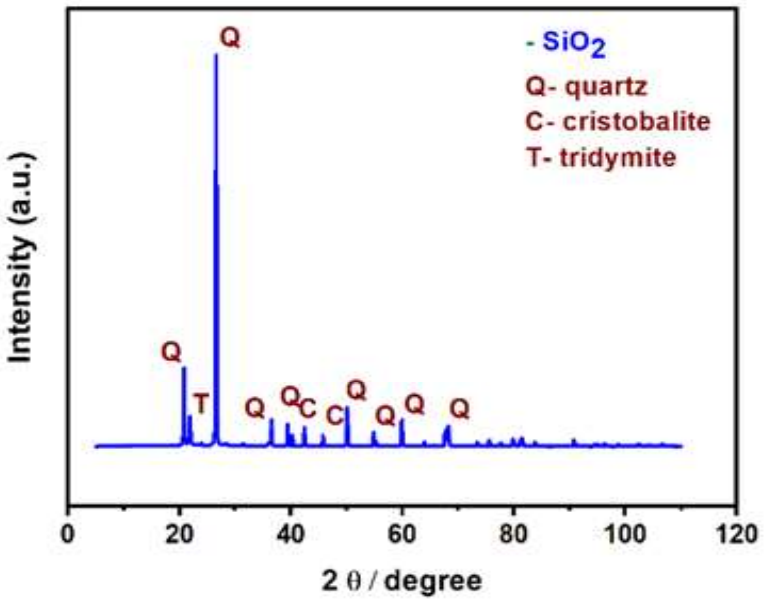

Fig. 4.8 XRD pattern of sintered silica foam

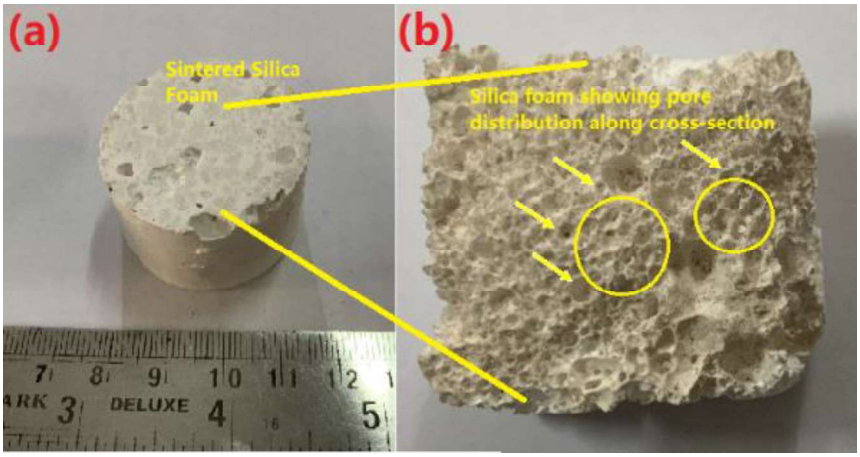

Fig. 4.9 Figure showing (a) silica foam sintered at 1500°C and (b) their pores distribution along the cross-section

Finally, the above explained synthesis mechanism and chemical changes during foaming can be more visualized and supported by FTIR and EDX data. Figure 4.10 shows the infrared spectra of the green and sintered silica foam, in the frequency range of 400-4000 cm^{-1}. The absorption bands at 461 cm^{-1}, 581 cm^{-1} and 615 cm^{-1} is due to the symmetric Si-O bending vibrations, whereas absorption bands located at 799 cm^{-1}, 851 cm^{-1} and 889 cm^{-1} are due to the asymmetric Si-O stretching vibrations. These vibrations arise from atomic motions within the SiO_4 tetrahedra [146]. The less intense O-H peak at 3450 cm^{-1} indicates partial dehydration of the sucrose by the concentrated sulphuric acid or due to adsorbed water vapour on the green silica foam. The absorption bands at 2416 cm^{-1} and 2616 cm^{-1} next to O-H band represent

aliphatic C-H vibrations. The peaks at wave numbers 1637 cm^{-1} most probably correspond to C=C stretches, indicative of aromatic groups. A new peak at 1878 cm^{-1}, corresponding to C=O vibration is observed after carbonization, which is possibly due to oxidation and esterification of the abundant O-H groups in sucrose by H_2SO_4 [147]. Sharp peaks in the region 1000-1300 cm^{-1}, corresponds to O=S=O, -SO_3H group and Si-OH group [148]. These strong sharp peaks confirm the carbonization and dehydration of sucrose by H_2SO_4. The presence of peaks at 504 cm^{-1}, 695 cm^{-1}, 621 cm^{-1}, and 799 cm^{-1} and disappearance of peaks in the region 1000-2900 cm^{-1} in the sintered sample suggest successful conversion of carbon coated silica foam into crystalline silica foam. Peaks at 504 cm^{-1}, 695 cm^{-1}, 621 cm^{-1}, and 799 cm^{-1} correspond to symmetric and asymmetric Si-O stretching vibration confirming the presence of silica in the sintered foam sample. Figure 4.11 (a) gives the elemental composition data of silica powder, clearly showing silica (Si) and oxygen (O) elements. The appearance of carbon (C) and sulphur (S) along with "Si" and "O" elements further approves the carbonization process of sucrose by sulphuric acid (Fig. 4.11 (b)). Figure 4.11 (c) again shows the presence of only two elements, "Si" and "O", in the sintered foamed samples. This confirms that the final foamed body is silica and all the impurities which are produced by dehydration reaction are removed during the calcination process.

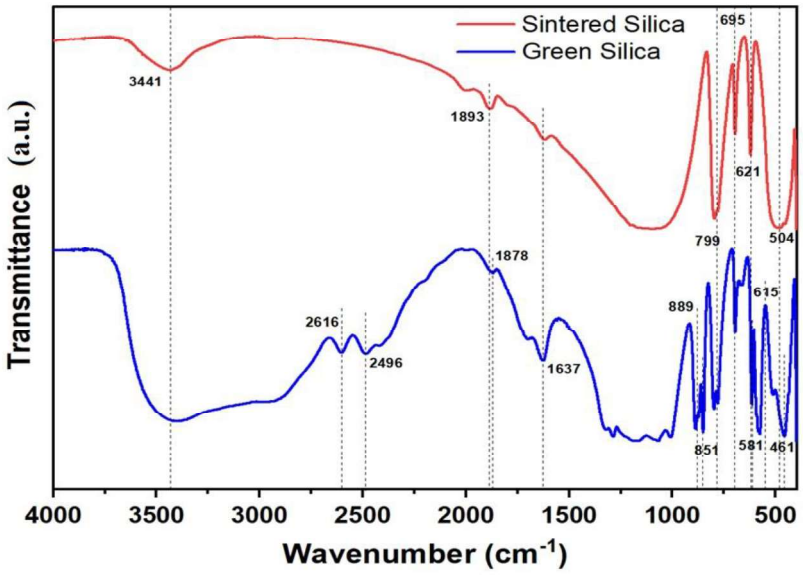

Fig. 4.10 FTIR pattern of green and sintered silica foams

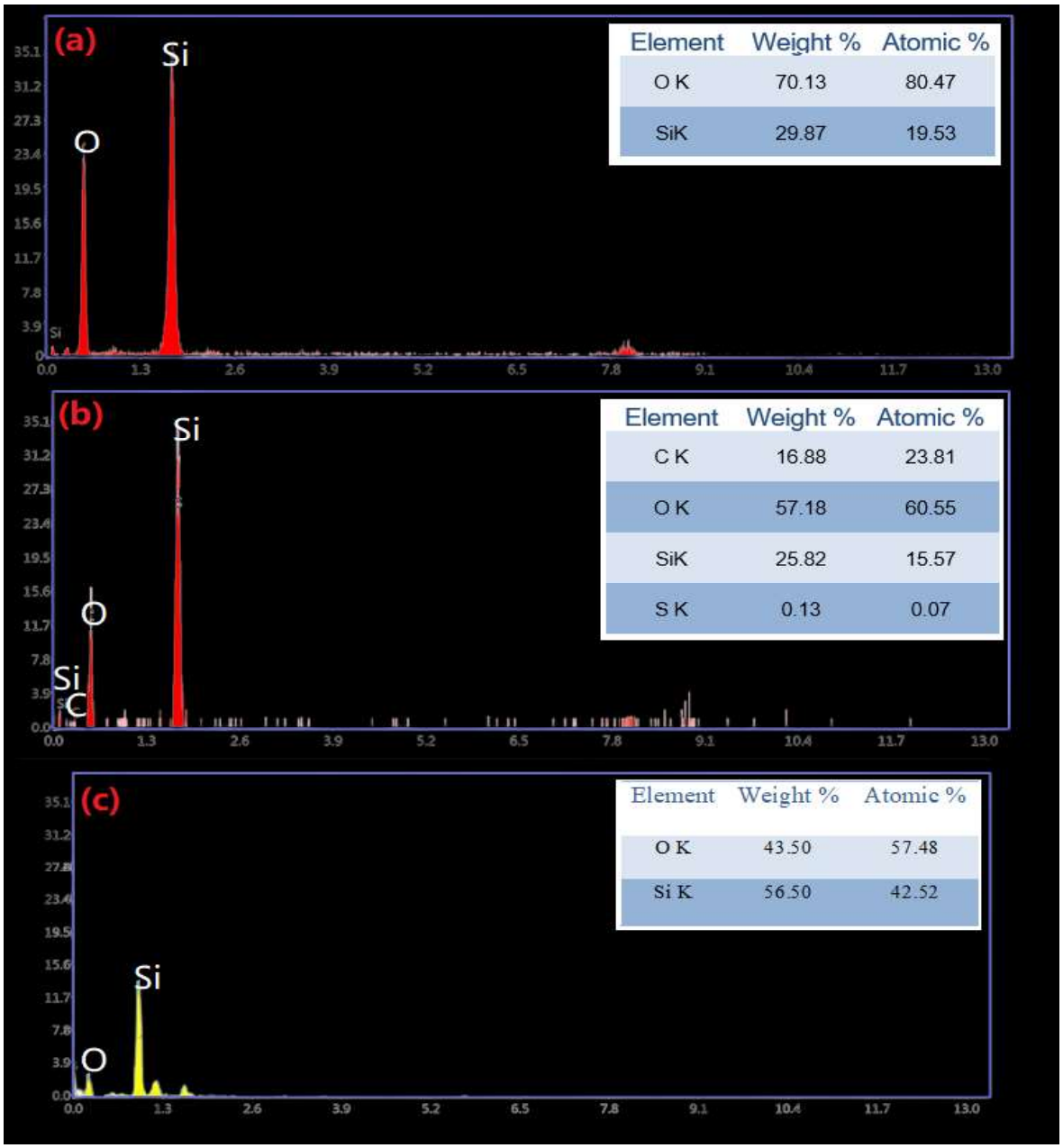

Fig. 4.11 EDS profile of (a) SiO_2 powder (b) Sulphuric acid treated sucrose- silica composition (c) Sintered silica foam

4.3.2 Microstructure of the Silica foams

SEM microphotographs and Micro-CT images of developed foams are obtained to investigate the microstructure details of silica foams. From the Micro-CT image of Fig. 4.12, it is revealed that the foam consists of several hundred microns of large pores and a few microns of thickness struts. Both closed and open pores are present in the foam. Open pores in the form of windows to the cell wall of closed pores ensures interconnectivity to the foam.

SEM reveals that reticulated structures with open and spherical pores have been formed due to the evolution of formed gases. Sucrose amount controls the microstructural development of the foam. Higher $W_{Su/Si}$ ratio leads to higher porosity with an increased number of pores but smaller pore diameter. This results in more connectivity among pores and makes them open. These open pores on the cell wall would improve the open porosity, making it easier to pass through any fluid or gas. An increase in porosity and the number of pores at a higher sucrose percentage can be ascribed to the evolution of excess gases that vigorously exert more pressure, thereby increasing the foam height and the number of windows. The above explanation also corroborates with the observations of SEM microstructures of the samples given in Fig. 4.13.

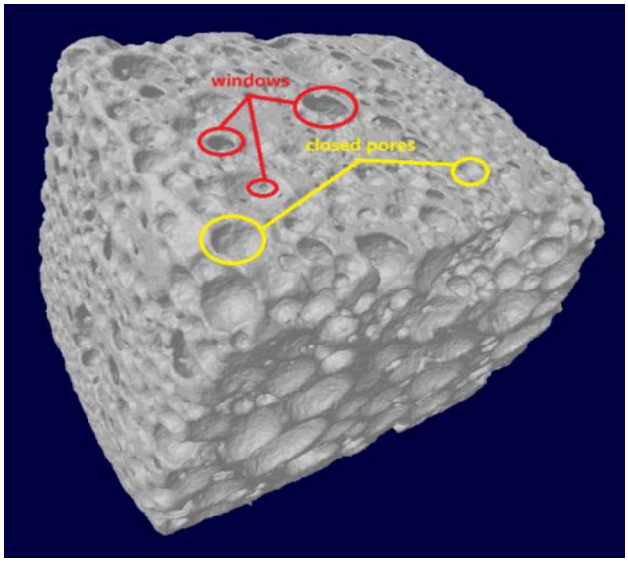

Fig. 4.12 Micro-CT image of silica foam prepared by sucrose dehydration process with 0.2 $W_{Su/Si}$ ratio and sintered at 1600°C

It is found that silica foams possess macropores, mostly spherical in shape with pore size in the range of 319-1021μm. The mean pore diameter of silica foams sintered at 1300°C is approximately 674μm when the $W_{Su/Si}$ ratio is 0.01, but the average pore size would decrease to 319μm when this ratio increases to 0.2. Conversely, an increasing trend is seen in average pore size when the sintering temperature has been increased to 1600°C. The mean pore diameter increases to 1021μm when the $W_{Su/Si}$ ratio is 0.01 and sintered at 1600°C. This fact explains that high sintering temperature helps consolidating smaller pores, which further leads to larger pores (Fig. 4.14). It is found that the pore structure homogeneity in silica foams is retained, but the pore size distribution varies slightly among the samples sintered at different temperatures. It is also worth to mention that the present procedure has the ability to create both open and closed pores. However, ratio of open to closed pore depends on sucrose to silica weight ratio as well as sintering temperature. As revealed in Table 2, higher open porosity up

to 50% (closed porosity 37%) can be achieved when using high $W_{Su/Si}$ ratio (0.2) and low sintering temperature (1300°C). Also, lower open porosity of 6% only can be achieved, when using low $W_{Su/Si}$ ratio (0.01) and high sintering temperature (1600°C). Table 2 provides details of various compositions used to prepare silica foam with their physical and microstructural data.

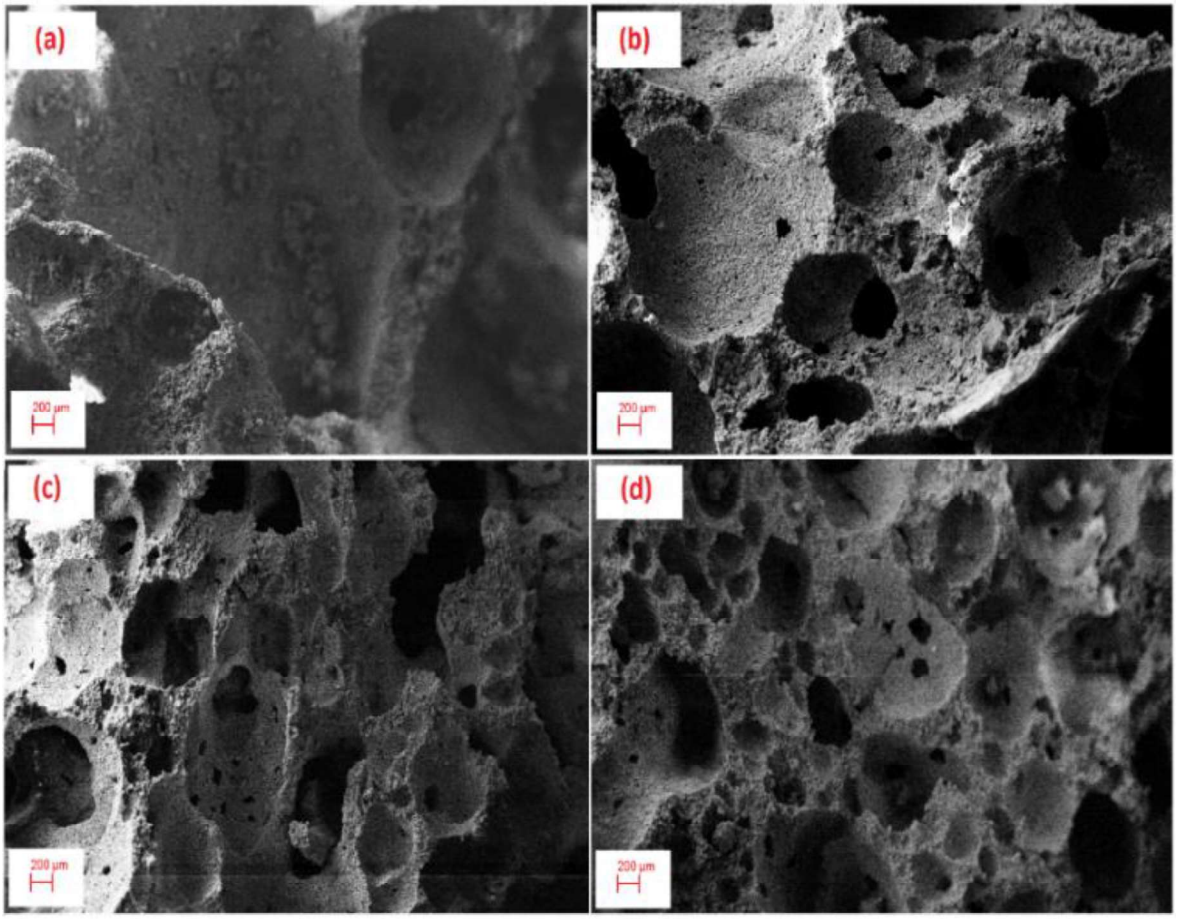

Fig. 4.13 SEM images of sintered silica foams prepared by sucrose dehydration with varied $W_{Su/Si}$ ratio: (a) 0.01 wt.%, (b) 0.05 wt.%, (c) 0.1 wt.%, (d) 0.15 wt.%. (Samples are sintered at 1300°C)

The obtained silica foams also possess good mechanical strength owing to their thicker strut size (Fig. 4.15). SEM micrographs revealed that the average strut size of foams lies in the range of 167.854-303.222µm. Average strut thickness decreases monotonically with increasing sintering temperature. The explanation for the above can be linked to the consolidation process during sintering which leads to the contraction of strut thickness. Furthermore, the $W_{Su/Si}$ ratio also positively impacts foam strut thickness. A reversing trend is observed for strut thickness with sucrose weight percentage as compared to sintering temperature. Silica foam sintered at

1300°C shows an average strut thickness of 251.327µm at 5wt % of sucrose. This is found to increase to 303.222µm when the sucrose percentage increases to 20wt %. The reason is that the decrease in the average pore size of foams with an increase in sucrose weight percentage creates space for the expansion of the struts. This might also lead to cracking in the struts of some samples as shown in Fig. 4.16. Cracks developed may be attributed to the insufficient gas pressure, which is unable to escape during the dehydration process or may be due to the sintering defect.

Table 4.2 Different Mixture Compositions, the Corresponding Microstructural Properties of Porous Silica Samples Fabricated Using Sucrose Dehydration Process

Sucrose to Silica weight ratio	Sintering Temperature (°C)	Bulk Density (g/cm^3)	Total Porosity (%)	Open Porosity (%)	Closed Porosity (%)	Average Pore Size (µm)	Average Strut Thickness (µm)	Average Strut Pore Size (µm)
0.01	1300°C	0.5353	79.8	39.3	40.5	674.1	251.327	5.489
0.05	1300°C	0.4346	83.6	40.2	43.4	666.7	257.357	5.423
0.10	1300°C	0.37895	85.7	44.4	41.3	499.2	267.159	5.134
0.15	1300°C	0.33655	87.3	47.9	39.4	465.1	289.753	5.023
0.20	1300°C	0.31535	88.1	50.2	37.9	319.2	303.222	4.998
0.01	1400°C	0.5591	78.9	29.4	49.5	711.3	165.458	5.03
0.05	1400°C	0.5247	80.2	30.6	49.6	705.4	171.857	5.1
0.10	1400°C	0.4558	82.8	33.9	48.9	505.5	188.258	4.68
0.15	1400°C	0.4081	84.6	38.2	46.4	447.8	206.753	4.32
0.20	1400°C	0.3604	86.4	40.7	45.7	393	278.875	4.159
0.01	1500°C	0.78705	70.3	9.4	60.9	729.45	161.324	4.075
0.05	1500°C	0.73405	72.3	10.5	61.8	721.5	168.234	4.435
0.10	1500°C	0.65985	75.1	13.5	61.6	598	172.854	3.975
0.15	1500°C	0.59625	77.5	17.1	60.4	489.6	179.215	3.876
0.20	1500°C	0.51145	80.7	19.8	60.9	429.7	184.754	3.654
0.01	1600°C	1.026	61.3	6.2	55.1	1021.9	149.857	2.047
0.05	1600°C	0.916105	65.43	6.6	58.83	1018	154.825	2.452
0.10	1600°C	0.87185	67.1	7.8	59.3	900.4	159.323	1.875
0.15	1600°C	0.8056	69.6	8.9	60.7	700.3	163.456	1.256
0.20	1600°C	0.7632	71.2	10.1	61.1	658.4	167.854	0.998

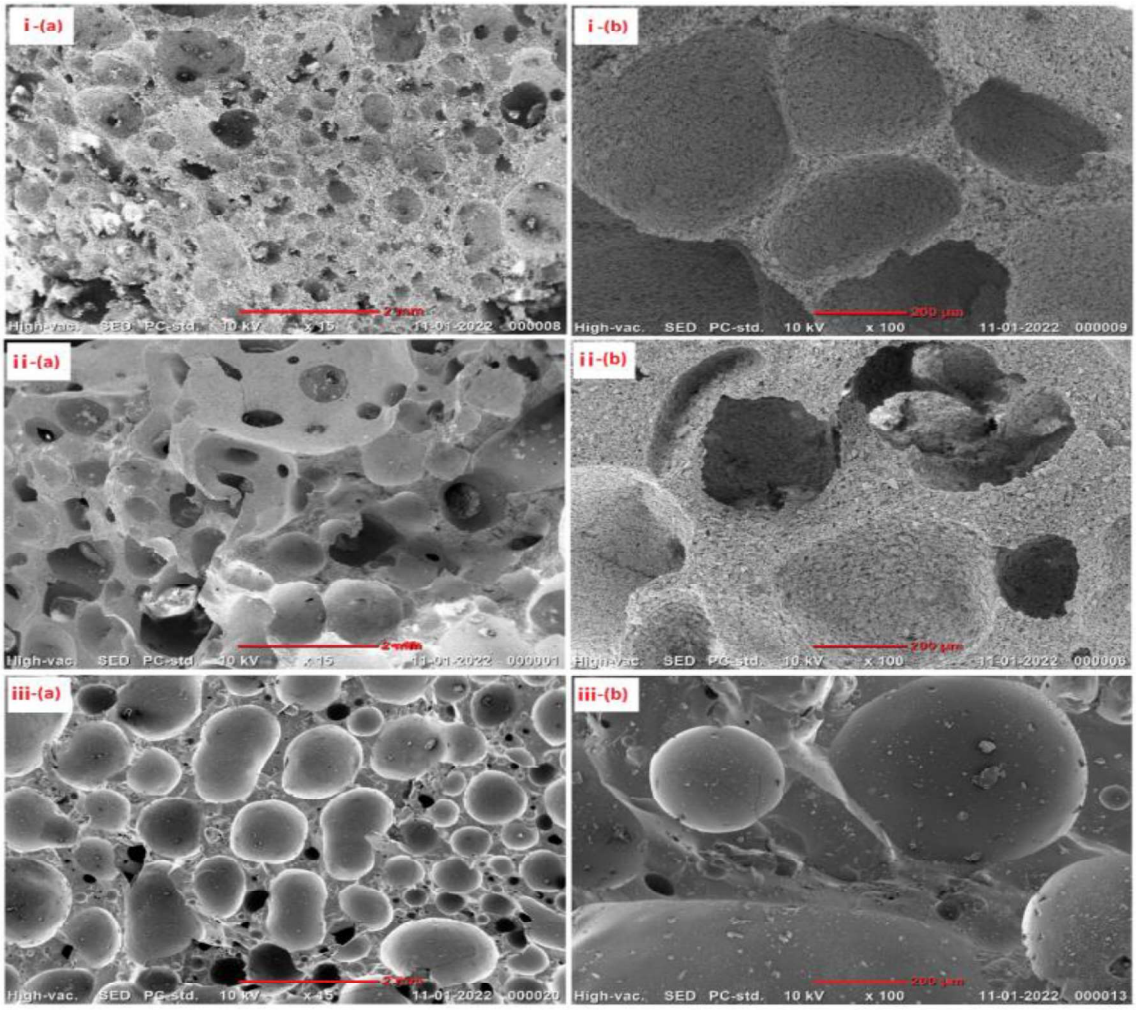

Fig. 4.14 SEM images of silica foams sintered at different temperatures: (i-a) 1300°C, (i-b) 1300°C, (ii-a) 1500°C, (ii-b) 1500°C, (iii-a) 1600°C, (iii-b) 1600°C. (Samples are prepared at 0.2 $W_{Su/Si}$ ratio)

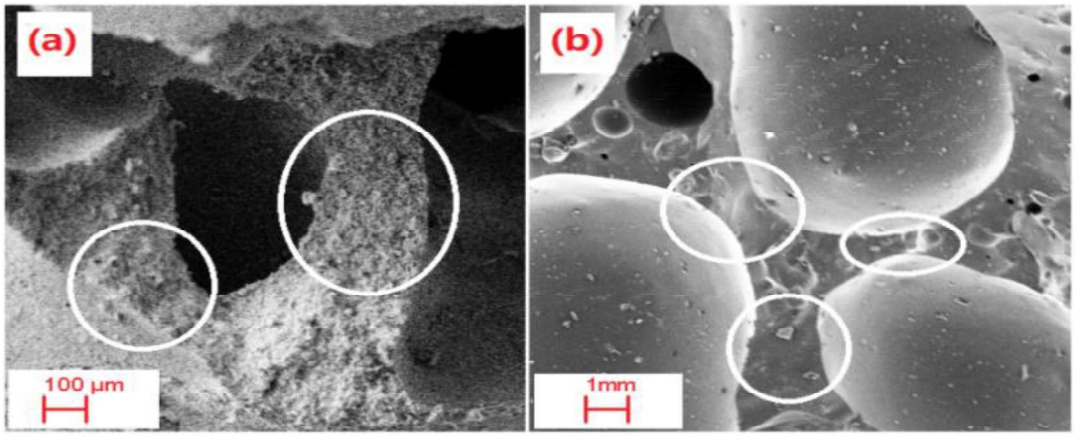

Fig. 4.15 SEM images of foam struts in the ceramic foam sintered at different temperatures: (a) 1400°C, (b) 1600°C. (Samples are prepared at 0.2 sucrose to silica weight ratio)

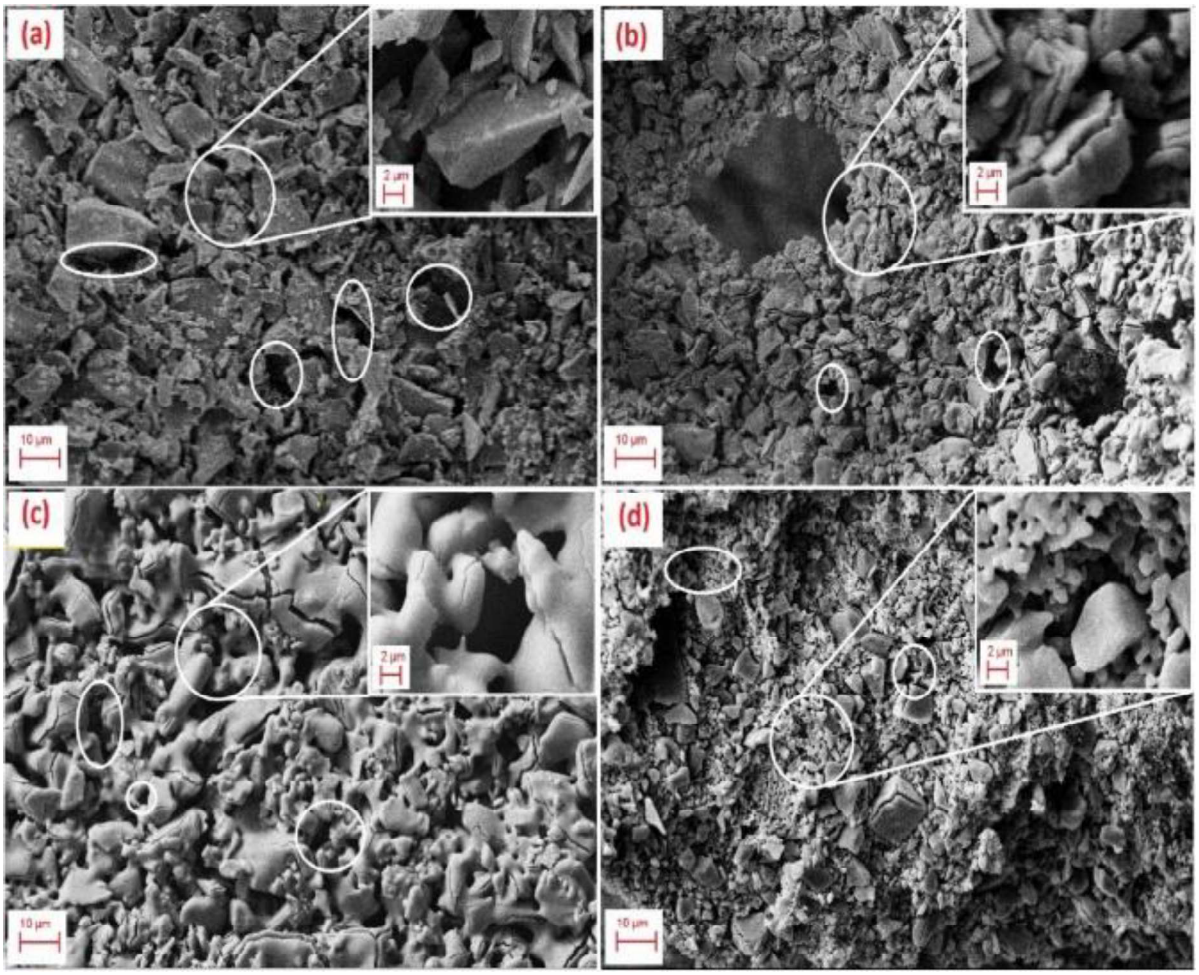

Fig. 4.16 SEM images of intercrystallite pores of sintered silica foams prepared by sucrose dehydration, sintered at different temperatures: (a) 1300°C, (b) 1400°C, (c) 1500°C, (d) 1600°C. (Samples are prepared at 0.2 sucrose to silica weight ratio)

One of the additional advantages of the as-fabricated silica foams is their intercrystallite pores, which provide extra porosity and discontinuity against thermal flow. The origin of these intercrystallite pores can be explained due to the gaseous pressure during foaming, creating space between the grains of the strut, which remains maintained during the consolidation process. This might also be due to the voids provided by agglutinated carbons during the heat treatment process. Most of these intercrystallite pores are closed ones. The authors believe that the closed porosity exhibited by these foams is primarily the effect of intercrystallite pores. The closed porosity of foams is determined to be in the range of 37.9 % to 55.1 %, obtained while subtracting open porosity from total porosity. Fig. 4.16 provides SEM micrograph showing intercrystallite pores in the strut part of silica foams.

4.3.3 Physical, mechanical, and thermal properties of the ceramic foams

Highly porous silica foams having 60-90% porosity have been fabricated successfully through the sucrose dehydration process. The obtained silica foams have a bulk density in the range of 0.3604-1.026 g/cm^3. Most of the foams having bulk density less than water show floatability property (Fig. 4.17).

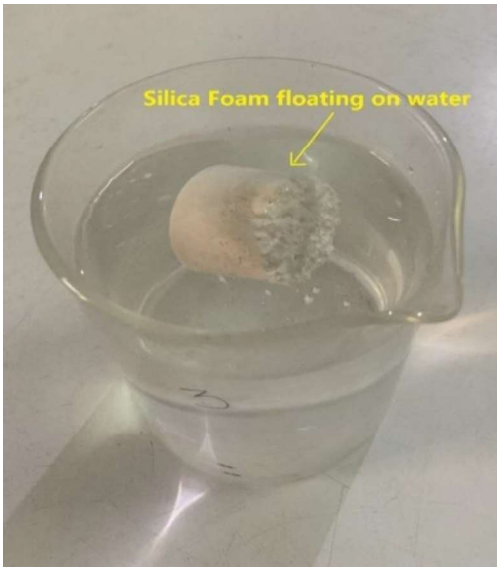

Fig. 4.17 Image of highly porous light weight silica foam floating in the water, showing floatability property

Fig. 4.18 shows the effect of $W_{Su/Si}$ ratio on the total porosity and average pore size of the silica foams. Total porosity increases linearly from 80% to 90% with the increase in sucrose weight percentage. This is because of availability of more sucrose amount for dehydration reaction at higher weight ratios. An addition of a mere 1% of sucrose amount into ceramic powder mixture is capable of generating ceramic foam with 80% total porosity. This further increases up to 90% with the increase in sucrose amount. However, a reversing trend is observed for average pore size, which decreases with the increase in sucrose amount. Average pore size observed for the foam samples prepared at 0.01 to 0.20 $W_{Su/Si}$ ratio are in the range of 1021.9-319.2 μm.

The compressive strength of the prepared foams are found to be in the range of 0.8 MPa to 2.8 MPa. Compressive strength decreases with the increase of $W_{Su/Si}$ ratio, but increases with the sintering temperature (Fig. 19(a)). This behaviour is attributed to the increase in number of pores in silica foam at a higher $W_{Su/Si}$ ratio and consolidation of foams at higher sintering temperatures. The stress-strain curve of silica foams sintered at 1500°C shows a multi-peak profile, typical of cellular ceramics (Fig. 4.19(b)) [149]. Initially, a positive slope is obtained up to the first breakdown of the foam showing maximum loading capability of the foam, which

abruptly falls down due to cracking (apparent stress drop), leading to a negative slope. However, an increase in stress load is further seen, showing foam can withstand higher loads that again fall after the second breakdown. This rise and fall in the stress curve during the strut crack cycle gives rise to the jagged stress-strain curve. Surface cracks with multiple branching are developed prior to the final crushing of the specimens (Fig. 4.20).

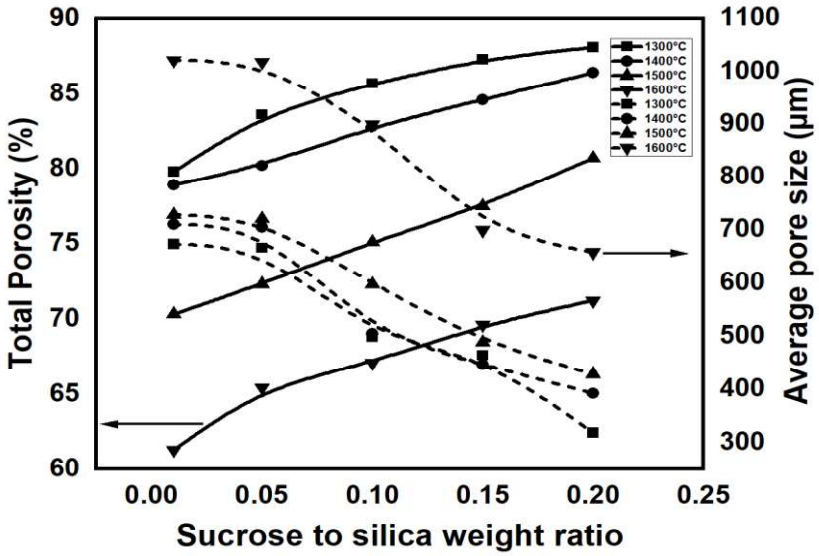

Fig. 4.18 Effect of sucrose to silica weight ratio on the total porosity and average pore size

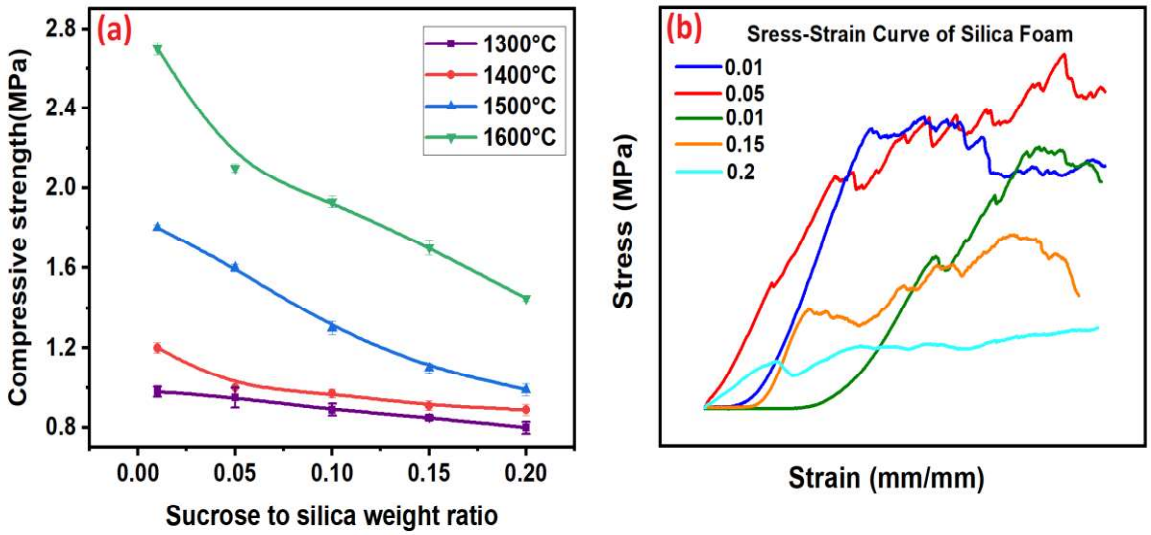

Fig. 4.19 (a) Effect of sucrose to silica weight ratio on the compressive strength of silica foam, (b) Stress-strain profile of silica foams

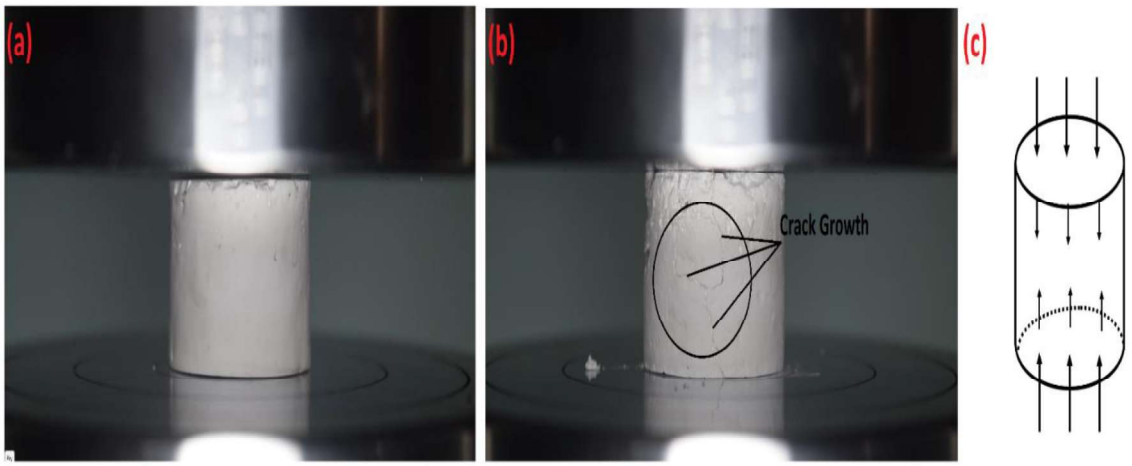

Fig. 4.20 (a) Silica foam before compression test, (b) Surface cracks developed in the silica foam during compression test, (c) Schematic drawing of the stresses involved in the compression testing

The present silica foams show good thermal resistant properties due to their extreme porosity. Thermal conductivity obtained is in the range of 0.0943-0.2571 $Wm^{-1}K^{-1}$. The bar chart in Fig. 21 demonstrates the dependence of thermal conductivity on porosity with a variation in the sintering temperature of foam specimen. Thermal conductivity is seen to decrease significantly with an increase in total porosity. This suggests that $W_{Su/Si}$ ratio is a very effective parameter for tailoring thermal conductivity. This trend is compatible with the total porosity of the silica foams. While increasing the sintering temperature, thermal conductivity is found to increase among the same group of specimens. Sintering temperature helps in the consolidation of silica particles which further decreases the total porosity. This decrease in total porosity increases the thermal conductivity of the silica foams. However, higher temperature also results in a more uniform spherical and closed pore, which helps in increasing thermal resistance. But the thermal resistance provided by closed pores is relatively less compared with the thermal conductivity increase due to a decrease in total porosity. So, the overall thermal conductivity increases with increasing sintering temperature. The obtained silica foams show comparable or even superior thermal resisting properties to products from other methods, giving the sucrose dehydration process an extra edge toward the low-cost formation of silica foams for thermal applications [137–140,143,150].

4.4 Comparative analysis and Cost analysis

Table 3 provides physical and mechanical properties comparison details of some of the methods available in the literature, albeit different procedures [142,143,151][47-55] to develop silica/ silica composite foams with the present findings. These Silica foams produced in different ways

possess porosity in the range of 32.83-91.35 % with compressive strength in the range of 0.27-20.54 MPa. It is also worth mentioning that only silica composite foams show more compressive strength than monolith porous silica foam. Further reinforcement provides better strength to silica foams. The near comparable and even in some instances, superior properties give impetus to the large-scale adoption of the proposed low-cost synthesis procedure to obtain silica foam. The foam specimens prepared exhibit sufficient porosity with mechanical and thermal properties within the applicable range as compared with other reported work.

Table 4.3 Physical and Mechanical properties of Silica foam/ Silica foam composites processed through various route.

Title	Synthesis method	Porosity range (%)	Compressive strength (MPa)
Present work	**Sucrose dehydration process**	**75-90**	**2.8-0.8**
Highly porous gelatine silica hybrid scaffolds with textured surfaces using new direct foaming/freezing technique [52].	Direct foaming/freezing	~90 vol%	1.77-0.27
Highly porous silica foams prepared via direct foaming with mixed surfactants and their sound absorption characteristics [53].	Direct foaming	84.6-91.35	5.89-0.94
Efficient synthesis of hollow silica microspheres useful for porous silica Ceramics [49].	Sacrificial template method	69.434	4.42
Porous silica ceramics with closed-cell structure prepared by inactive hollow spheres for heat insulation [54].	Spray drying and plasma sintering	74.16-80.25	5.4-2.0
Fabrication of porous silica ceramics by gelation-freezing of diatomite slurry [51].	Gelation-freezing method	52-90	-
Effects of polysiloxane on thermal conductivity and compressive strength of porous silica ceramics [48].	Dry compaction	70.3-76.4	14.5-3.9
Fabrication and properties of silica/mullite porous ceramic by foam-gel casting process using silicon kerf waste as raw material [50].	Foam-gel casting	32.83-74.72	20.54-3.60
A facile green chemistry route to porous silica foams [47].	Low-temperature hydrothermal ion-exchange reaction	70.1	11.9-4.1
Porous silica ceramics with relatively high strength and novel bi-modal pore structure prepared by a TBA-based gel-casting method [55].	Gel-casting process	70.1-72.4	5.82-4.38

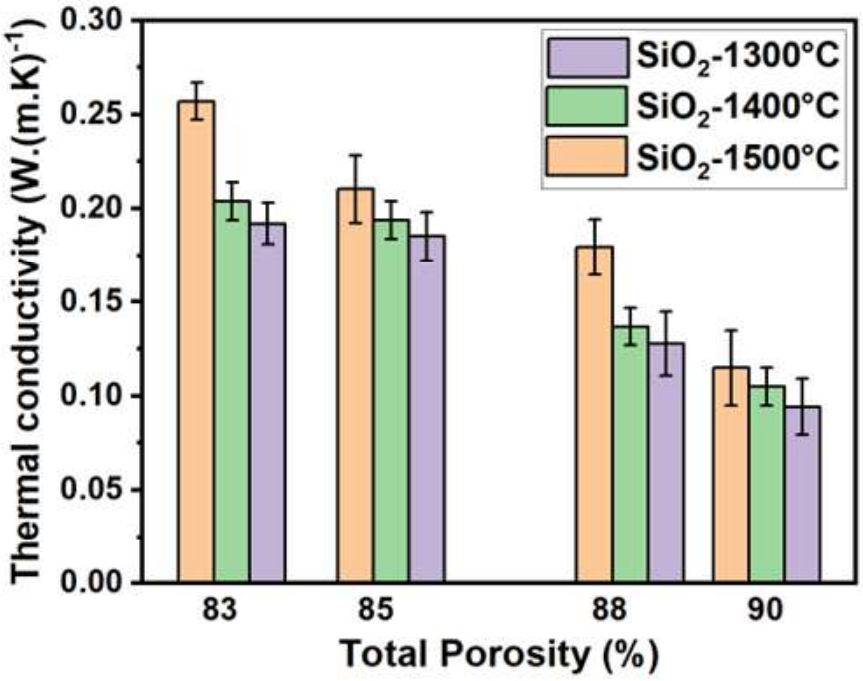

Fig. 4.21 Effect of total porosity on thermal conductivity of silica foams

Table 4.4 Cost analysis of the prepared silica foam.

Raw materials	**Unit price (₹/kg)**	**Amount used per silica foam [10*10*5-15 cm^3] (g)**	**Cost per silica foam (₹)**
Silica Powder	20	95-80	1.9-1.6
Sucrose	38	5-20	0.19-0.76
Sulphuric Acid (98%)	14	60	0.84
Total raw material cost per silica foam			₹2.63-3.5
Approximate cost of shaping and sintering at 1400 °C for 2h (based on the power rating of the furnace and unit electricity price).			₹48/sample
Estimated total cost			$0.69-0.702/sample

*Currency conversion used (USD to INR): $1 = ₹73.36

Silica, which is abundant, low-cost and readily available, is the major constituents of the raw materials used for fabricating the silica foam. Table 4.3 provides detailed cost analysis of the raw materials involved in fabricating 10×10×(5-15) cm^3 sized silica foam. The raw material cost for developing the specified volume of silica foam comes around approximately ₹2.63-

3.5. The cost for green synthesis and sintering at 1400˚C comes around ₹48/sample. This makes the estimated overall cost of developed silica foam around ₹50.63-51.5/sample ($0.69-0.702), which is very competent and makes the above dehydration process a cost-effective way towards ceramic foam processing.

4.5 Conclusions

A novel, reaction generated thermo-foaming synthesis route has been incorporated in this work for the first time to produce silica foam using sucrose dehydration process with sulphuric acid. Sucrose is used both as a blowing agent as well as fugitive material, along with sulphuric acid, which facilitates in inducing foaming effect inside the ceramic slurry for the development of silica foam. Foam height and cell interconnectivity are directly influenced by the $W_{Su/Si}$ ratio. Enough pores are seen to be developed by the evolution of gases produced during the dehydration process. The porosity of the developed silica foam has been tailored by varying the amount of sucrose in the ceramic mixture. Apart from closed pores generated due to the thermo-foaming process, open channels in the form of windows are also present in pore walls due to excess gaseous pressure in the slurry. The presence of intercrystallite pores within the struts can be attributed to the burnout of agglutinated carbon from silica particles and subsequent partial sintering. These intercrystallite pores provide extra resistivity to heat flow and thus enhance the thermal insulating properties.Employing the described process, high-porosity silica foam specimens are fabricated successfully by varying $W_{Su/Si}$ ratio and controlling the amount of sulphuric acid and sintering temperature. The obtained silica foam possesses porosity up to 90% with reasonable thermo-mechanical properties. The presence of both open pores and intercrystallite pores in the developed foam makes it suitable for a wide range of applications such as catalyst supports, filters, bioscaffolds and such other thermal applications in different fields. So, the procedure outlined might emerge as a low-cost process for developing equivalent strength ceramic foams for potential thermomechanical applications.